Supplementary Information (SI) for Chemical Science.

Supporting Information

Iron-Assisted Growth of Anisotropic ZnO Nanostructures

Zhengxi Xuan,[ab] Avisek Dutta,[cd] Shuo Liu,[ag] Yueling Qin,[f] Kaiwen Chen,[a] Zheng Fu,[ab] Paras N. Prasad,[cd] Chaochao Dun,*[g] and Mark T. Swihart*[ab]

[a] Department of Chemical and Biological Engineering, University at Buffalo, The State University of New York, Buffalo 14226, NY, USA

[b] RENEW Institute, University at Buffalo, The State University of New York, Buffalo 14226, NY, USA

[c] Department of Chemistry, University at Buffalo, The State University of New York, Buffalo 14226, NY, USA

[e] Department of Chemistry, Institute for Lasers, Photonics, and Biophotonics, The State University of New York, Buffalo 14226, NY, USA

[f] Department of Physics, University at Buffalo, The State University of New York, Buffalo, New York 14260, United States

[g] The Molecular Foundry, Lawrence Berkeley National Lab, Berkeley, CA 94720, USA

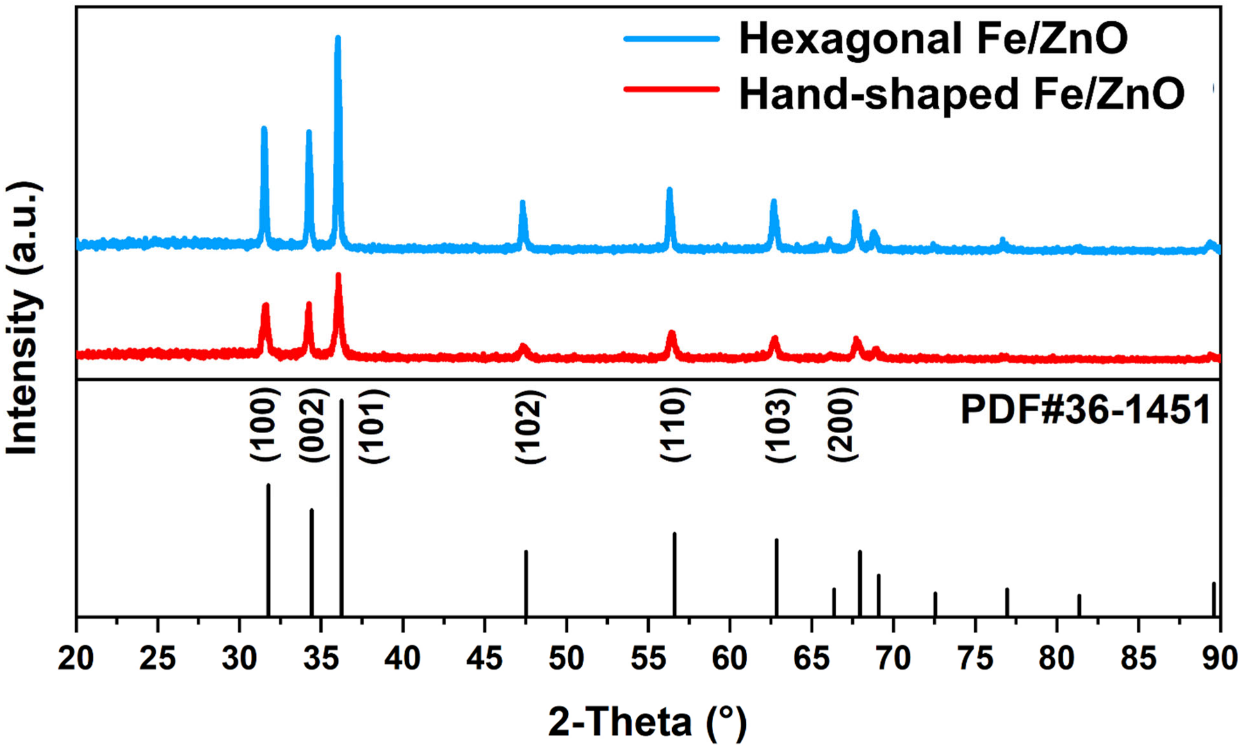

Fig. S1 XRD patterns of hand-shaped and hexagonal Fe/ZnO nanostructures.

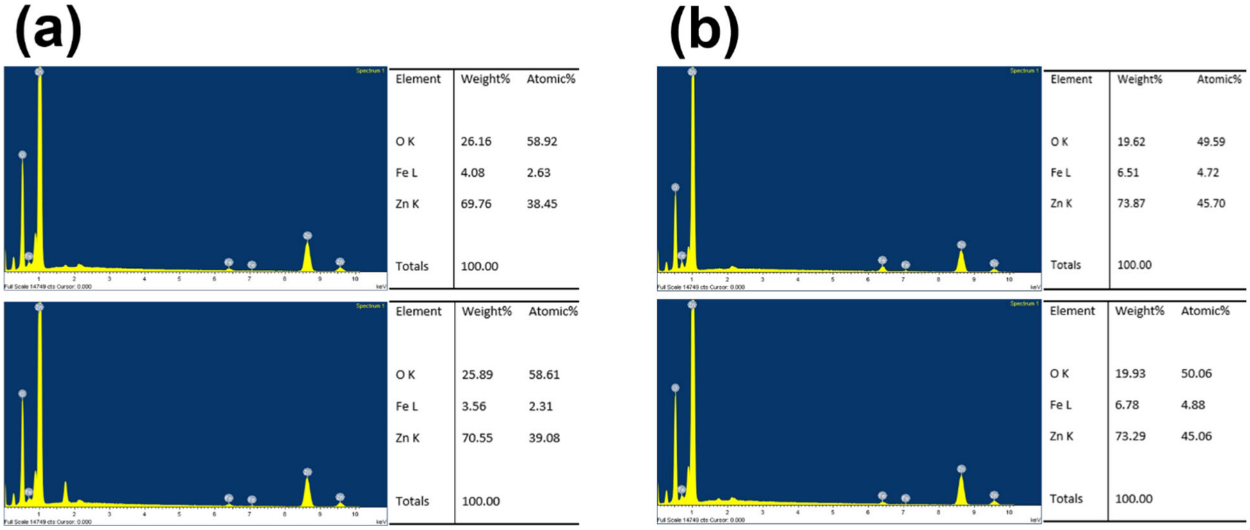

Element	Weight%	Atomic%
O K	26.16	58.92
Fe L	4.08	2.63
Zn K	69.76	38.45
Totals	100.00	

Element	Weight%	Atomic%
O K	25.89	58.61
Fe L	3.56	2.31
Zn K	70.55	39.08
Totals	100.00	

Element	Weight%	Atomic%
O K	19.62	49.59
Fe L	6.51	4.72
Zn K	73.87	45.70
Totals	100.00	

Element	Weight%	Atomic%
O K	19.93	50.06
Fe L	6.78	4.88
Zn K	73.29	45.06
Totals	100.00	

Fig. S2 SEM-EDS elemental analysis for (a) hand-shaped and (b) hexagonal Fe/ZnO nanostructures. Results for two sites on each sample are shown.

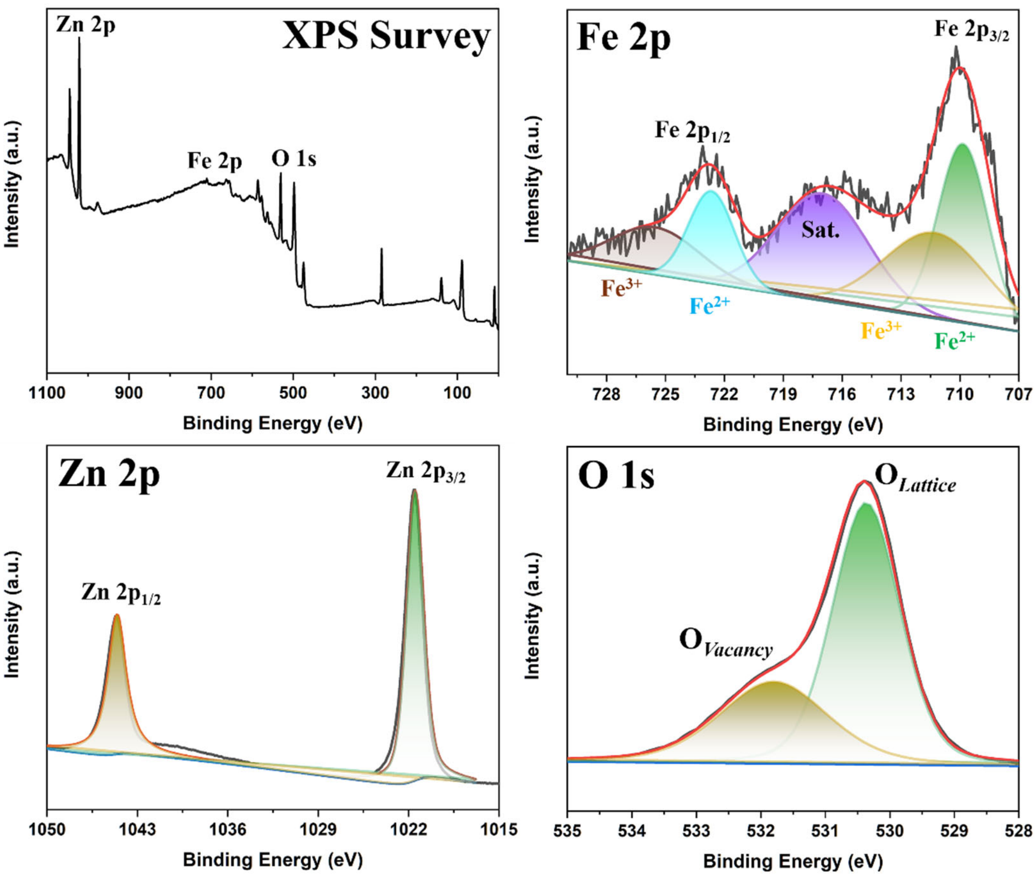

Fig. S3 XPS spectra for hand-shaped Fe/ZnO nanostructure.

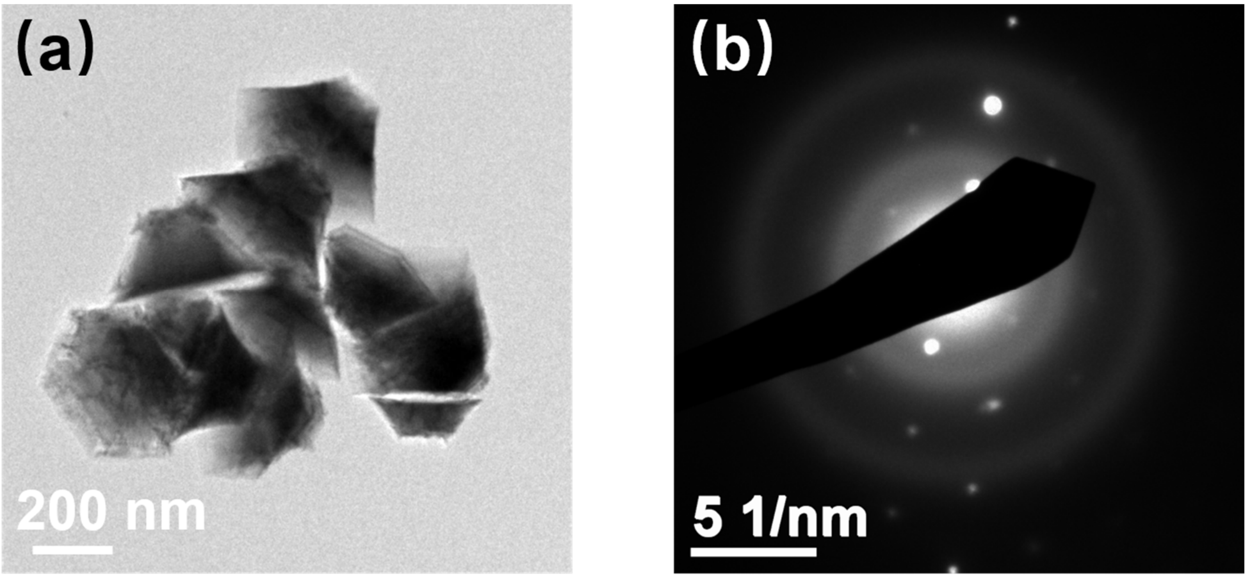

Fig. S4 (a) TEM image for hexagonal Fe/ZnO nanostructures and (b) corresponding SAED pattern.

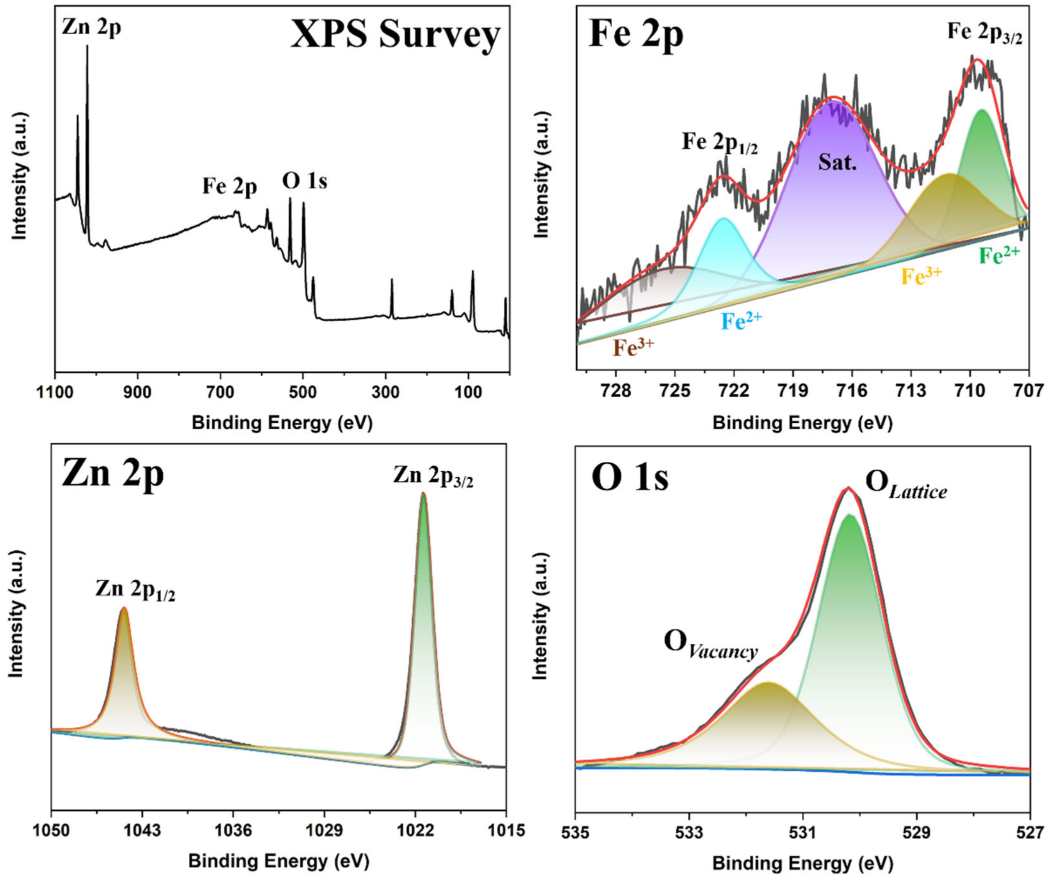

Fig. S5 XPS spectra for hexagonal Fe/ZnO nanostructure.

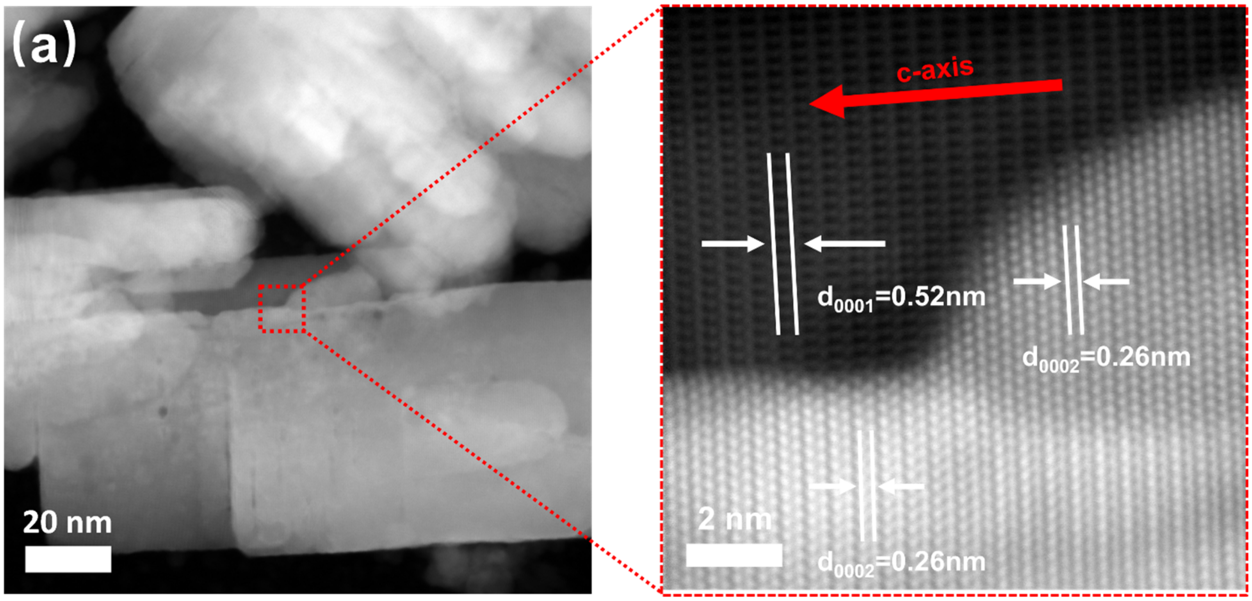

Fig. S6 (a) HAADF-STEM and (b) atomic-resolution HAADF-STEM images of hand-shaped Fe/ZnO nanostructures.

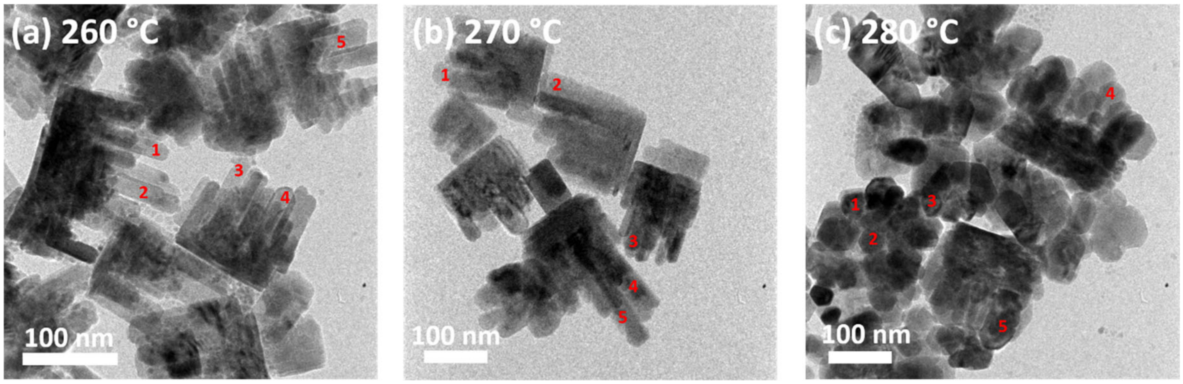

Sites #	Diameter (nm)		
	(a) 260°C	(b) 270°C	(c) 280°C
1	18	35	43
2	18	34	42
3	16	26	36
4	22	40	41
5	20	36	48
Average	19	34	42

Fig. S7 and Table. S1 Diameter profiles at selected sites of hand-shaped Fe/ZnO nanostructures prepared at (a) 260°C, (b) 270°C and (c) 280°C.

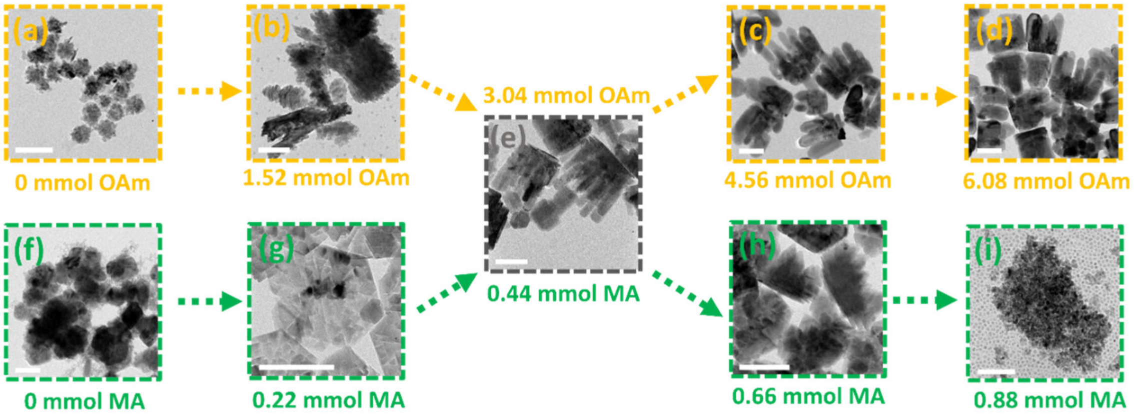

Fig. S8 TEM atlas of morphology control in hand-shaped Fe/ZnO nanostructures by varying amounts of (a)-(e) oleylamine and (e)-(i) myristic acid. The amounts of ligands employed are specified under the TEM images. Scale bars are 100 nm.

Ligand Effects on Growth of Hand-shaped Fe/ZnO Nanostructures. Surface ligands play an important role in guiding the formation of the Fe/ZnO hand-shaped nanostructures. Fig. S8† illustrates the shape evolution of these nanostructures when making minor adjustments to the quantities of ligands used during synthesis. Reaction conditions of Fig. S8e† were employed using 3.04 mmol OAm, 0.44 mmol MA and final reaction temperature of 270 °C as the base conditions. Fig. S8a-e† presents samples for which only the amount of OAm was varied, while Fig. S8e-i† show samples with changes in the amount of MA, while the remaining reaction conditions remain unchanged. Specifically, in Fig. S8a†, the sample without OAm exhibits a porous, pinecone-like morphology.[1] Increasing the concentration of OAm promotes Fe doping into the ZnO lattice;[2, 3] and at 3.04 mmol OAm, the typical hand-shaped structure begins to form. A 50% increase (Fig. S8c†) and 100% increase (Fig. S8d†) in OAm concentration further stabilized the Fe/ZnO hand-shaped nanostructures, similar to the effect of increasing temperature, promoting growth. However, we note that MA also plays a synergetic role with the OAm in promoting the growth of these hand-shaped nanostructures. In Fig. S8f†, the absence of MA leads to ZnO nanostructures of irregular shape. The addition of 0.22 mmol MA (Fig. S8g†) results in hexagonal plate-like ZnO structures, similar to those seen in reactions conducted at 250 °C (Fig. 2f), with an “edge-up” configuration. In contrast, excess MA (Fig. S8g†) led to the formation of crown-like nanoparticles where pyramid-shaped fingers form instead of rod-like ones. Further increasing the concentration of MA (Fig. S8i†), yielded a secondary phase of iron oxide dots, with fewer products collected by centrifugation (See experimental methods for details). To study the composition of the surface ligands, FTIR measurements were performed. The FTIR spectra in Fig. S9† reveal mixed ligands on the surface. The distinct peak at 1737 cm^{-1} arises from C=O stretching, confirming the presence of MA[4, 5] while the peaks at 1566 cm^{-1}, due to N-H bending, and at 1227 cm^{-1}, due to C-N stretching, demonstrate the presence of OAm.[6, 7]

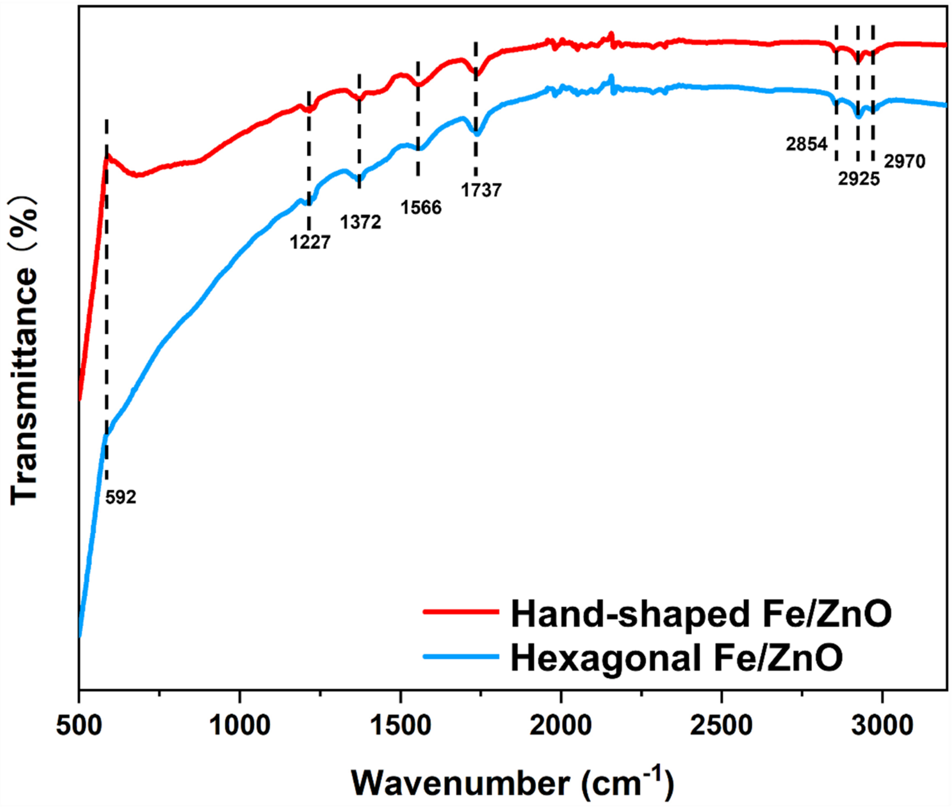

Fig. S9 FTIR spectra of hand-shaped Fe/ZnO and hexagonal Fe/ZnO nanostructures.

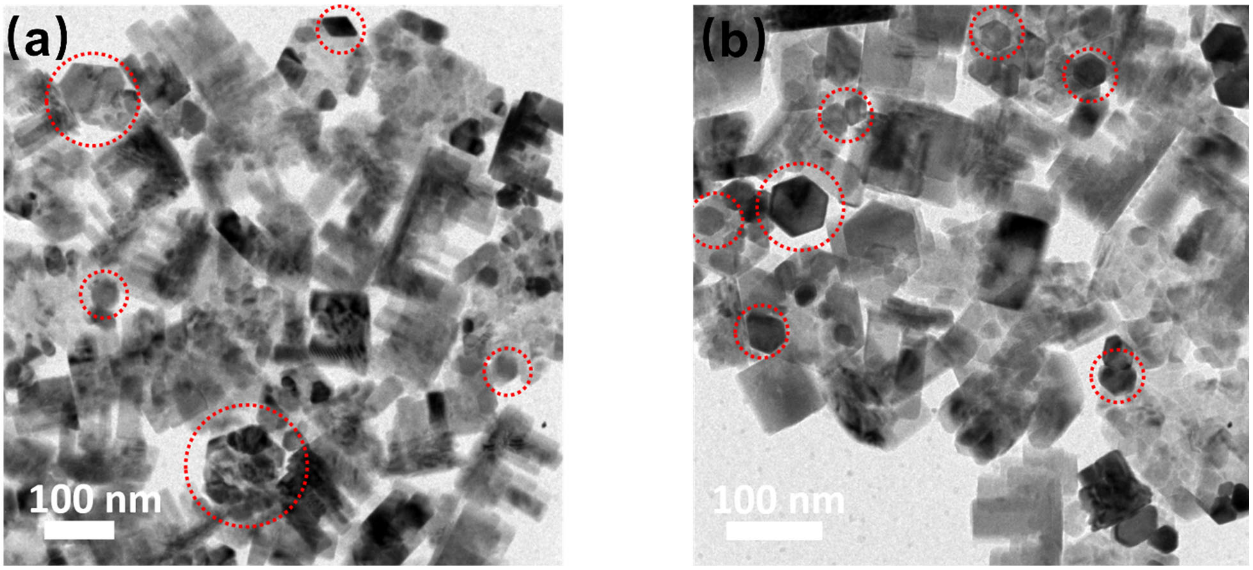

Fig. S10 TEM images for resulting hand-shaped nanostructures when (a) double and (b) triple amount of both iron and zinc precursors.

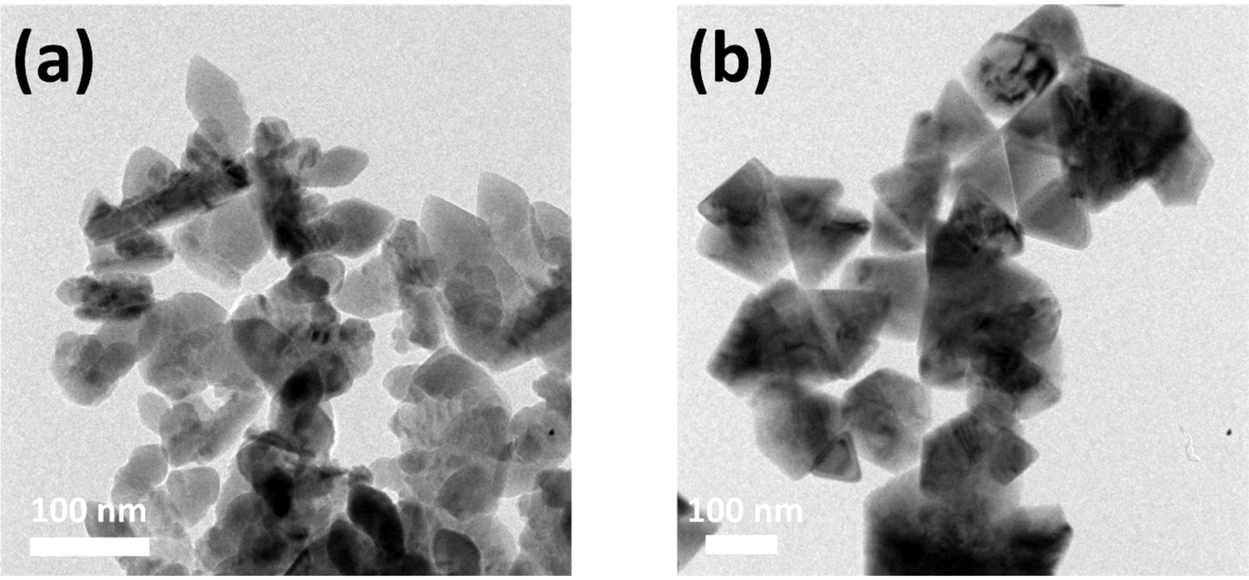

Fig. S11 TEM images for undoped (a) hand-shaped and (b) hexagonal ZnO nanostructures.

For the undoped hexagonal ZnO nanostructures, a small "gap" is visible between some paired nanostructures, suggesting the presence of an organic interfacial layer which would be expected from a ligand-based coupling. Additionally, SEM images (Fig. S12) reveal a lack of perfect morphological symmetry between the coupled nanostructures. Specifically, the lateral edges and exposed facets do not exhibit mirror symmetry with respect to the O-rich crystal planes. The asymmetry suggests that the nanostructures did not grow epitaxially from a common basal plane. Previous combined experimental and simulation studies have demonstrated similar tail-to-tail coupling behaviours driven by ligand-ligand interactions. Overall, these observations strongly suggest that the tail-to-tail coupling is mainly driven by ligand-ligand rather than the doping process.

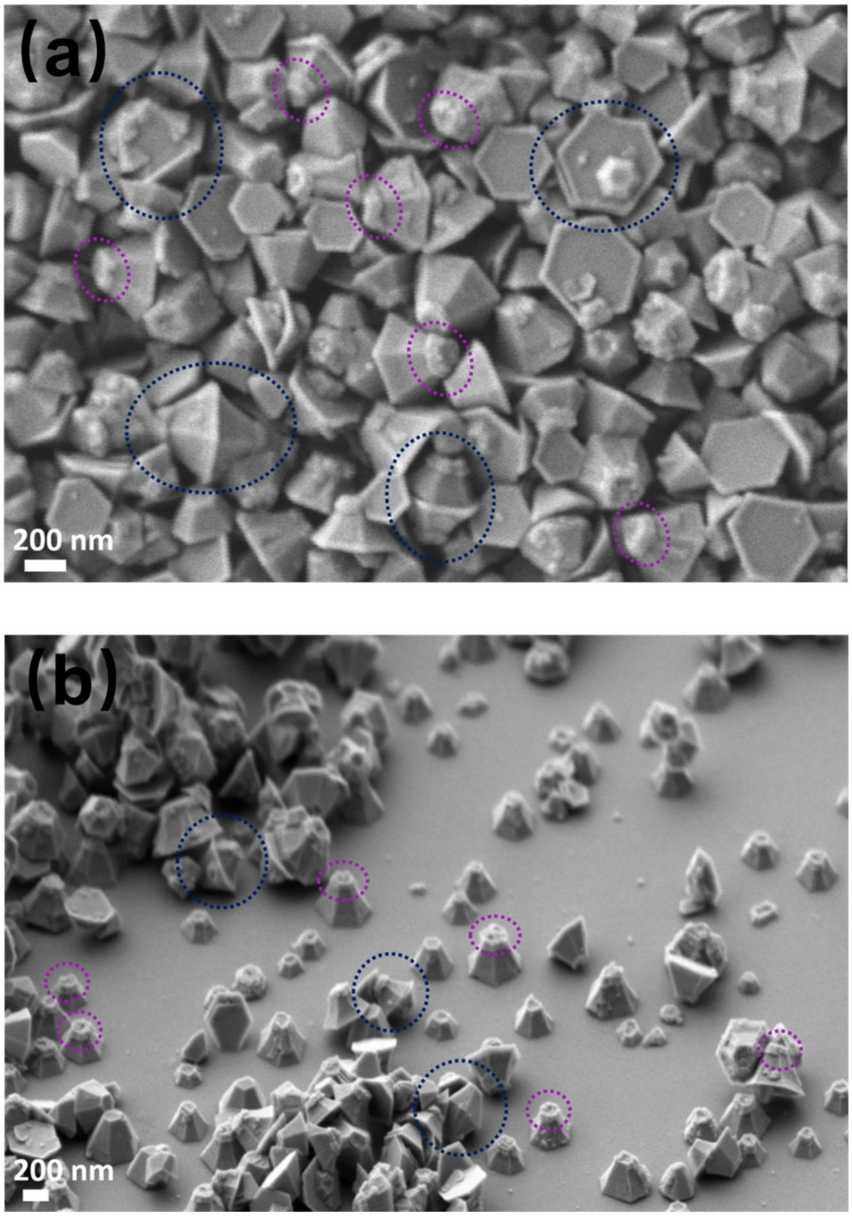

Fig. S12 SEM images of hexagonal Fe/ZnO nanostructures imaged with (a) 0 tilt angle and (b) 36 degree tilt angle on the SEM stage.

Table. S2 Diameter profiles of selective sites of hexagonal Fe/ZnO nanostructures corresponding to Fig 4. (f)-(i).

Figure 4.	Ratio between outer layer and whole particle		
	#1	#2	#3
(f)	0.047	NA	NA
(g)	0.066	NA	NA
(h)	0.253	NA	NA
(i)	0.241	0.201	0.169

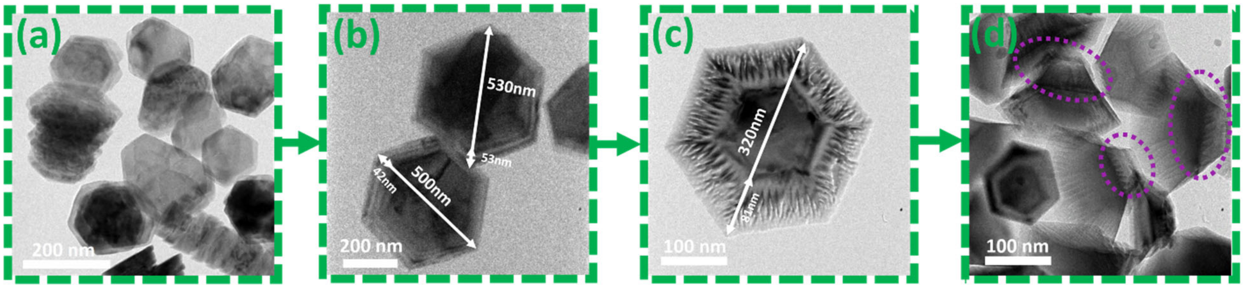

0 mmol MA　0.22 mmol MA　0.66 mmol MA　0.88 mmol MA

Fig. S13 TEM atlas of morphology-control in hexagonal Fe/ZnO nanostructures by varying the amount of myristic acid. The amount of ligand used is specified under the TEM images. (c) was reproduced from Figure 4h.

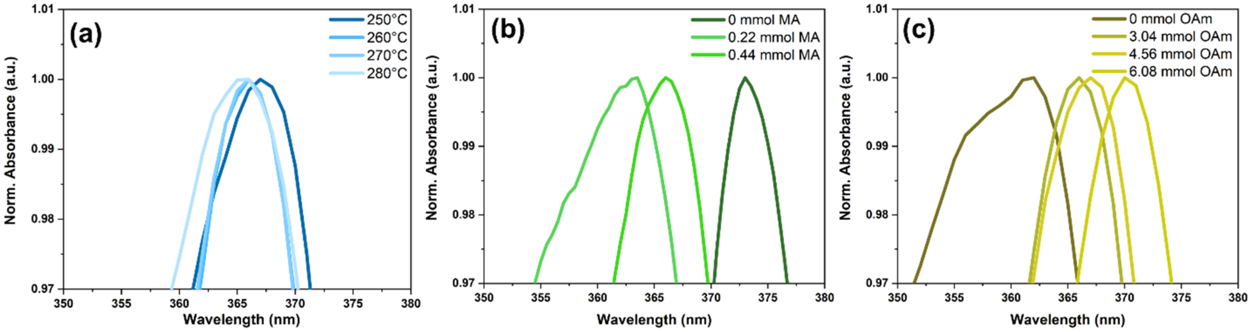

Fig. S14 Normalized UV-Vis spectra of hand-shaped Fe/ZnO nanostructures synthesized at various reaction parameters of (a) temperature, (b) myristic acid and (c) oleylamine.

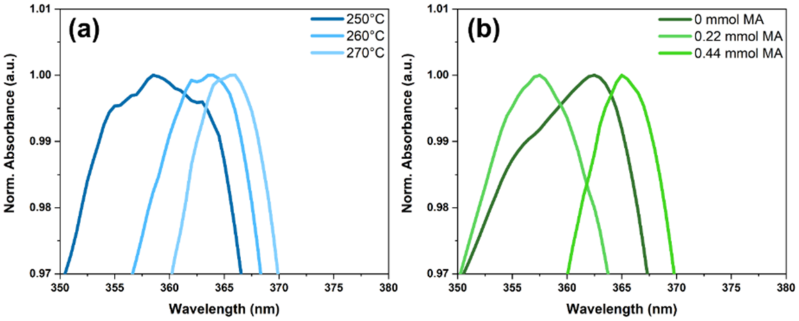

Fig. S15 Normalized UV-Vis spectra of hexagonal Fe/ZnO nanostructures synthesized at various reaction parameters of (a) temperature and (b) myristic acid.

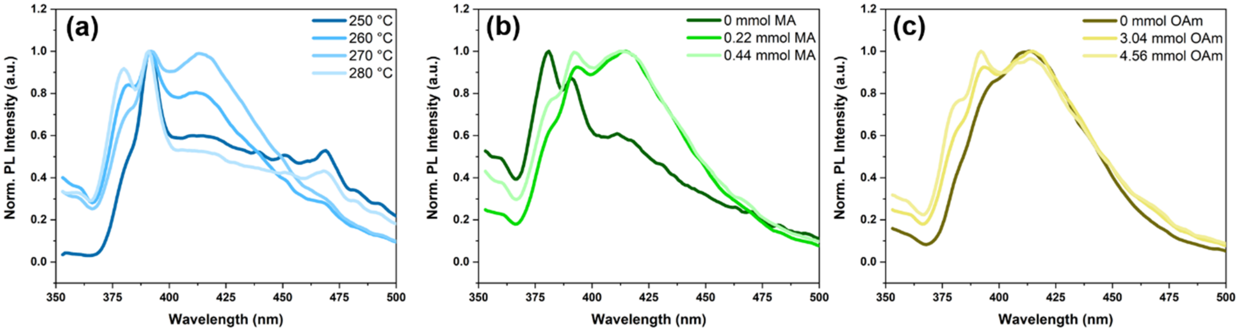

Fig. S16 Normalized PL spectra of hand-shaped Fe/ZnO nanostructures synthesised at various reaction parameters of (a) temperature, (b) myristic acid and (c) oleylamine.

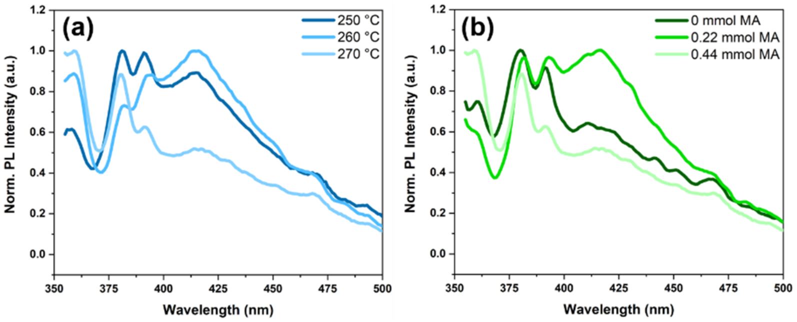

Fig. S17 Normalized PL spectra of hexagonal Fe/ZnO nanostructures synthesised at various reaction parameters of (a) temperature and (b) myristic acid.

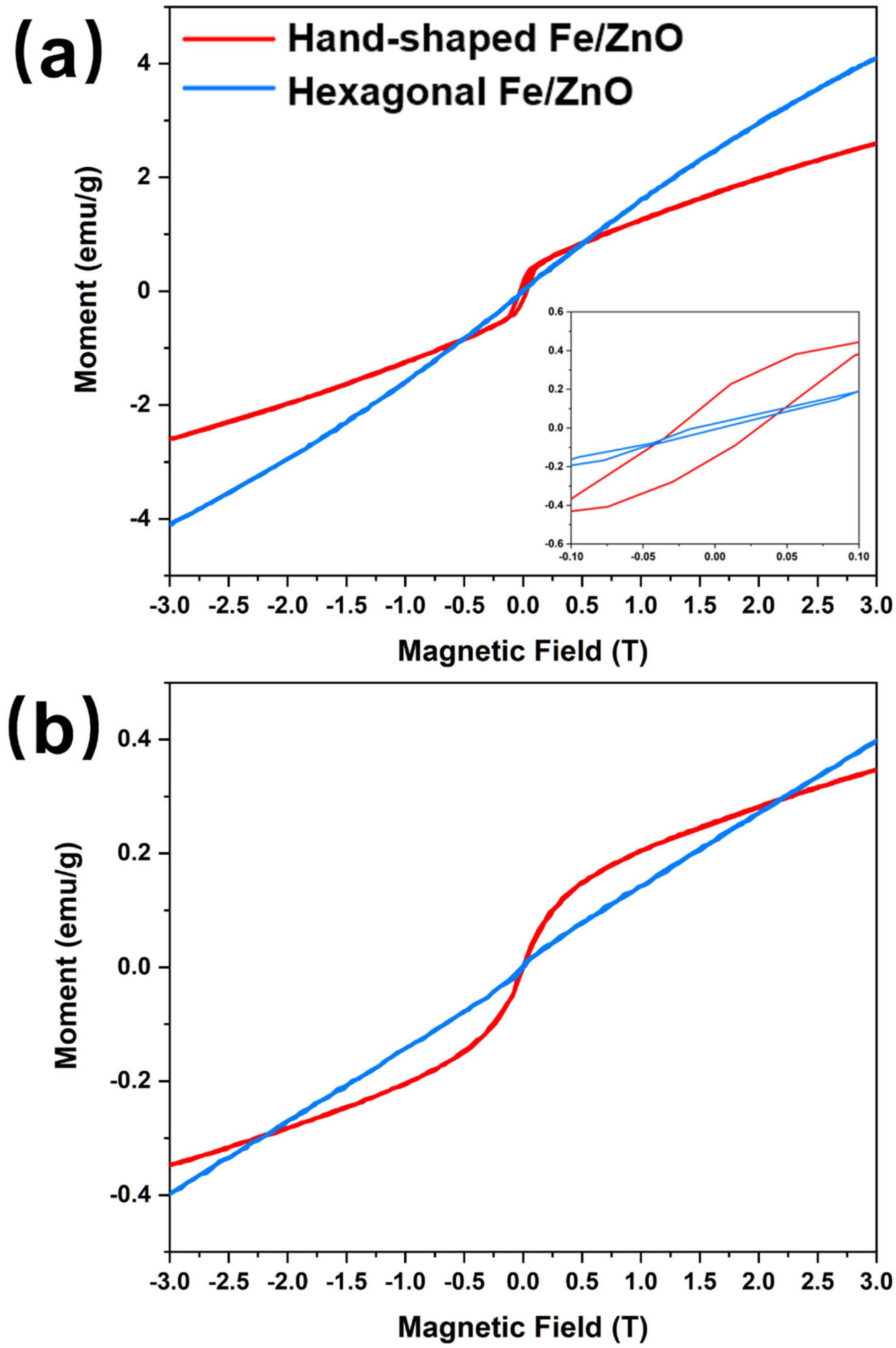

Fig. S18 Magnetic hysteresis for Fe/ZnO nanostructures measured at a) 8 K and b) 300 K.

REFERENCES

1. X. Liu and M. T. Swihart, *Nanoscale*, 2013, **5**, 8029-8036.
2. X. Li, Y. Liu, J. Song, J. Xu and H. Zeng, *Small*, 2015, **11**, 5097-5104.
3. P. Wainer, O. Kendall, A. Lamb, S. J. Barrow, A. Tricoli, D. E. Gomez, J. van Embden and E. Della Gaspera, *Chemistry of Materials*, 2019, **31**, 9604-9613.
4. C. Li, Q. Li, R. Ge and X. Lu, *Chem Eng J*, 2023, **458**, 141355.
5. D. Zhou, J. Yuan, Y. Zhou and Y. Liu, *Scientific Reports*, 2020, **10**, 10889.
6. K. Chang, C. Podder and H. Pan, *ACS Applied Nano Materials*, 2023, **6**, 23418-23429.
7. I. A. Safo, C. Dosche and M. Özaslan, *ChemPhysChem*, 2019, **20**, 3010-3023.